

Magneto-mechanical actuation of bonded ferromagnetic fibre arrays

A.E. Markaki, T.W. Clyne *

Department of Materials Science and Metallurgy, Cambridge University, Pembroke Street, Cambridge CB2 3QZ, UK

Received 1 June 2004; received in revised form 22 October 2004; accepted 27 October 2004

Available online 23 November 2004

Abstract

Strongly bonded assemblies of metallic fibres constitute an interesting class of highly porous, permeable materials. A high degree of control can be exercised over their properties, by tailoring the fibre architecture so as to achieve specified void contents, fibre connectivity and fibre orientation distributions. There is also scope for introducing controlled heterogeneity and gradient structures. It is possible, by using relatively strong fibres, and generating appropriate fibre–fibre joint geometries, to produce material with relatively high tensile strength and toughness, facilitating usage in various load-bearing applications. Furthermore, if ferromagnetic fibres are employed, then the material can be actuated by the imposition of a magnetic field, with the fibres becoming magnetised along their length and tending to align parallel with the applied field. The resultant deformation of the fibre array generates a shape change, which can be predicted for a given fibre orientation distribution and fibre segment aspect ratio (inter-joint distance over fibre diameter). Moreover, a non-magnetic (matrix) material located in the inter-fibre space will be mechanically strained by these fibre deflections. This was proposed in a previous publication as a possible mechanism for bone growth stimulation by magnetic field application, for example by making the surface layers of a prosthetic implant from a ferromagnetic fibre array, into which bone cell growth would occur. In the present paper, analyses are presented for prediction both of conventional elastic constants exhibited by bonded fibre arrays and of novel magneto-mechanical elastic constants. These analyses also allow identification of conditions for the onset of inelastic behaviour. Comparisons are made with experimental data, relating to nominally isotropic fibre arrays, with and without the presence of relatively compliant matrices. It is confirmed that a simple modelling approach can give fairly reliable indications of how the material will behave, under both mechanical and magnetic loading.

© 2004 Acta Materialia Inc. Published by Elsevier Ltd. All rights reserved.

Keywords: Metal fibres; Ferromagnetism; Elastic constants; Porosity; Magneto-mechanical induction

1. Introduction

There is strong interest [1–6] in highly porous metals, for a wide range of applications. Such materials encompass both closed-cell and open-cell geometries. An interesting class of materials, forming a sub-set of the latter group, is that made by assembling a set of slender members, such as metallic fibres, wires, rods, ribbons, etc., and bonding them together in some way, for example by welding, brazing, sintering or adhesive bonding.

These assemblies normally incorporate very high void contents, typically in the range 75–98%. Such materials can be further sub-divided according to whether the spatial location and orientation distribution of the individual members are regular or stochastic. The scale of the individual members can also cover a wide range. In fact, some such assemblies, made up of relatively coarse rods or struts and having a geometrically well-defined architecture, would commonly be classified as structures, rather than materials. In other cases, some sort of intermediate classification might be considered appropriate.

Such “quasi-materials” are worthy of more intensive study than they have received hitherto, since they can exhibit interesting characteristics. Of course, the

* Corresponding author. Tel.: +44 1223 334332; fax: +44 1223 334567.

E-mail address: twc10@cam.ac.uk (T.W. Clyne).

mechanical efficiency of various strut assemblies, such as trusses, and design techniques for the creation of high flexural rigidities, etc., have been well-known to mechanical engineers for a very long time, but clear translation of such concepts into the design of highly porous materials is not so advanced. Furthermore, the high surface-to-mass ratio of bonded fibre arrays means that they can be attractive in terms of transport phenomena characteristics, leading to applications involving heat transfer, filtration, catalyst support, acoustic damping, etc. The presence of high aspect ratio members also has the potential to confer interesting magnetic characteristics (see below). Finally, techniques available for the manufacture and processing of bonded fibre arrays are often well-suited to the production of strong inter-fibre joints and to tailoring of the void content and fibre orientation distribution (and controlled gradations of these). Such tailoring can encompass three-dimensional geometry, which is problematic with conventional (long fibre) composite materials. Bonded fibre arrays thus offer more potential for the creation of material with good mechanical strength and toughness than can be expected with other types of highly porous material.

There have been several previous studies of the mechanical characteristics of bonded fibre arrays [7–13]. The work of Gibson and Ashby concerned with modelling of open cell foams [14,15] can be applied to fibre arrays (see Section 3.1.2). Delannay and co-workers [12] measured the elastic constants of transversely isotropic steel fibre assemblies and also developed analytical models [13,16] for these. Delince and Delannay [13] presented a model based on a periodic network architecture, but found that predicted Young's moduli were below measured values. They attributed this largely to neglect in the model of triangulation effects. A model accounting for this effect has recently been developed [16].

There have also been several studies of the strength and toughness of bonded fibre arrays, both in tension and under compression. Ducheyne et al. [8] measured the (tensile) strength of sintered stainless steel fibre mats to be several tens of MPa. Theoretical study [17,18] of the compressive failure of such materials has usually led to the conclusion that local yielding, followed by plastic buckling of struts, is the critical process. A model has been developed by Markaki and Clyne [10] for the tensile fracture energy of bonded fibre arrays, utilising experimental data for the failure characteristics of single fibres.

A recent paper by Markaki and Clyne [6] introduced the concept that an array of ferromagnetic fibres will deform under the influence of an applied magnetic field, as individual fibres tend to align with the field. It was suggested that this effect might be utilised to stimulate bone growth, since bone tissue growing into such a porous array would be strained when a field was applied, with potential physiological benefits. An analytical model was presented for prediction of the induced deforma-

tion, together with experimental validation for single fibres and for small 4-fibre assemblies.

In the present paper, a simple rationale is presented for prediction of mechanical and magneto-mechanical characteristics of non-periodic bonded fibre assemblies having specified fibre orientation distributions, with and without the presence of a (relatively compliant) matrix.

2. Experimental procedures

2.1. Material and specimen production

Cylindrical specimens were produced by assembling short fibres, together with some braze powder. The fibres employed were of 446 alloy (ferritic stainless steel), $\sim 100\ \mu\text{m}$ diameter and $\sim 4\ \text{mm}$ long, produced by Fibretech using a melt extraction process. The porous specimens were created by spraying a small quantity (a few grams) of fibres with a (slow setting) aerosol glue and then sprinkling some braze powder (less than a gram) over them. The braze powder used, which is non-magnetic, has a composition (wt%) of Ni–14Cr–4Fe–2.8B–3.3Si–0.6C and was supplied by Brazing and Soldering Automation Ltd. The fibres, with braze particles adhering to them, were packed into a 250-mm long quartz tube of 16 mm internal diameter, with the fibres being repeatedly tamped down after progressive additions. The quartz tube was then evacuated, while being warmed slightly to drive off the residual glue, and sealed off. Brazing was carried out by holding at 1200 °C for a few minutes.

Material produced in this way had porosity levels of about 75–90%. A typical fibre content and distribution is illustrated by the scanning electron micrograph shown in Fig. 1. Some X-ray tomography has also been carried out to explore fibre orientations. The procedure outlined above generates a transversely isotropic distribution. While it is clear that the distributions produced were not fully isotropic, the tendency for fibres to lie in-plane was not predominant, with many fibre segments lying at relatively low θ values.

Some fibre arrays were infiltrated in vacuum with a low viscosity resin (Epofix, Struers) or a rubber (Evergreen™ 20, Smooth-On Inc.). The resin or rubber was poured onto the sample and, on admitting air to the chamber, was forced into the interstitial spaces between fibres. To ensure complete penetration, several pumping-venting cycles were conducted. Curing then took place at room temperature.

2.2. Mechanical loading

Cylindrical specimens of the bonded fibre array material, with or without surrounding matrix (resin or rub-

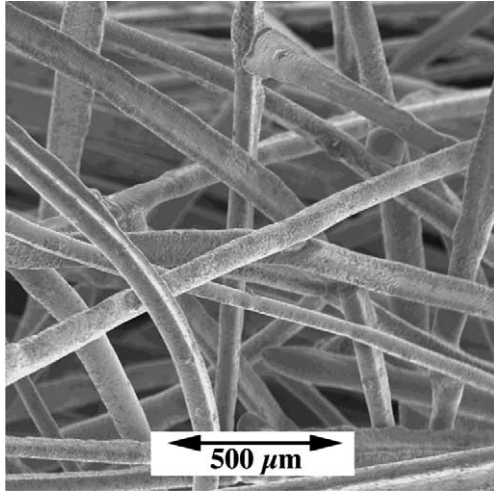


Fig. 1. Scanning electron micrographs of a bonded fibre array material, made by brazing short ferritic stainless steel fibres.

ber), and of the matrices themselves, were produced, each about 15 mm long and about 14 mm in diameter. These were loaded in axial compression on a servo-hydraulic testing apparatus equipped with a 1 or 10 kN load cell. The tests were conducted under displacement control, with a cross-head speed of 0.2 mm min^{-1} . The axial displacement was measured both via a LVDT and with a clip gauge extensometer. The axial stiffness was measured from the tangent of the unloading curves, within the elastic regime.

2.3. Magnetic loading

Cylindrical specimens of the bonded fibre array material with or without surrounding matrix (resin or rub-

ber) were magnetically actuated by being placed between the pole pieces of a water-cooled DC electromagnet (Helmholtz coil), with the field direction parallel to the axis of the specimen. The set-up is shown schematically in Fig. 2. The uniform field region was about 50 mm in diameter and 30 mm in length. The maximum field strength was about 1.2 Tesla. Dimensional changes were measured using a scanning laser extensometer (Lasermike), with a resolution of about $1 \mu\text{m}$.

3. An analytical model based on fibre bending

A simple analytical model has been developed, based on the bending of individual fibre segments (sections between joints). These act like pairs of cantilever encastré beams, joined at segment mid-points. It is assumed that the net deflections and strains within the fibre array are dominated by such fibre bending, so that the straining associated with conventional elastic stretching or compression of the fibres in the loading direction can be neglected. This is expected to be an acceptable approximation provided the segments are relatively slender. The corresponding lower limit on the segment aspect ratio is not well-defined, but by analogy with known characteristics of the bending of short beams, it is expected to be about 3. A nomenclature listing is presented as Appendix A.

3.1. Mechanical loading

The loading situation is depicted schematically in Fig. 3, focussing on the elastic deformation exhibited

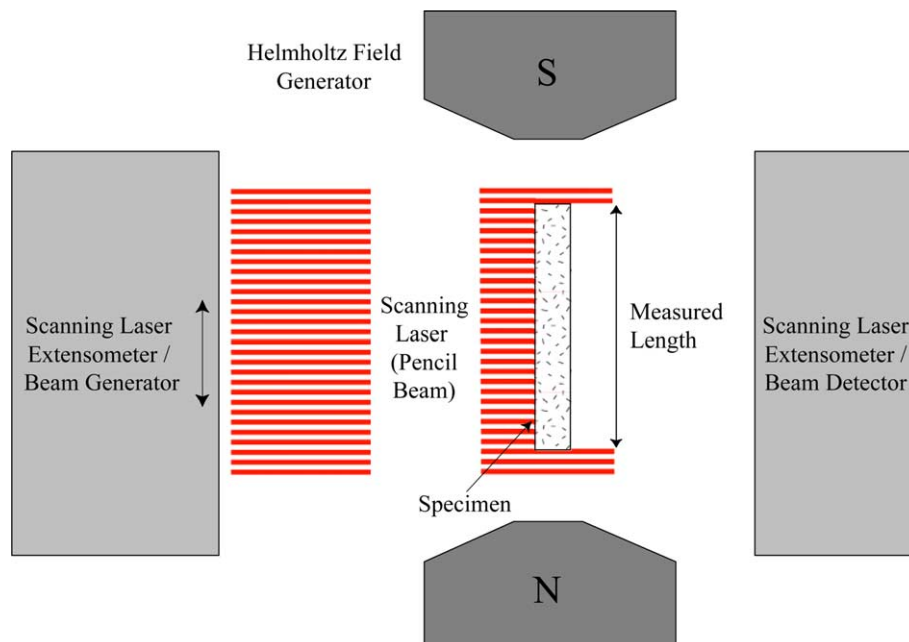


Fig. 2. Schematic depiction of the experimental set-up for monitoring specimen distortion under the influence of an applied magnetic field, *B*.

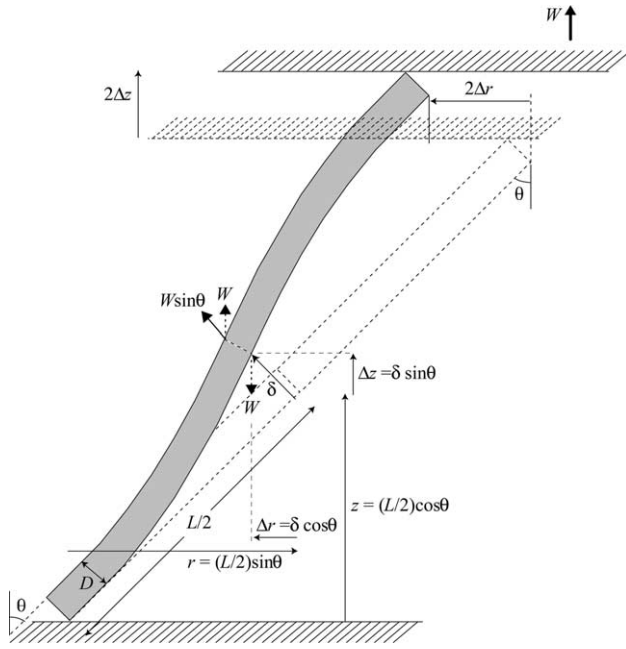


Fig. 3. Schematic representation of the deflection of a fibre segment within a fibre array, under the influence of an applied force, W .

by a single fibre within an array, lying with its axis at an angle θ to the loading direction. When a uniaxial stress is applied, a force W acts on each fibre in the loading direction, generating a bending moment.

3.1.1. Individual fibre deflections

The standard formula for the deflection, δ , at a distance x along an end-loaded cantilever beam, of length $L/2$, subjected to a force $W \sin \theta$ normal to the axis of the beam (see Fig. 3), may be written

$$\delta = \frac{(W \sin \theta)}{6E_f I} \left(3 \left(\frac{L}{2} \right) x^2 - x^3 \right), \quad (1)$$

where E_f is the fibre Young's modulus and I is the moment of inertia of the fibre section in bending, given by

$$I = \frac{\pi D^4}{64}, \quad (2)$$

where D is the fibre diameter. The deflection of the end of such a fibre ($x = L/2$) is thus given by

$$\delta = \frac{W \sin \theta (L/2)^3}{3E_f \left(\frac{\pi D^4}{64} \right)} = \frac{8W \sin \theta L^3}{3E_f \pi D^4}, \quad (3)$$

or, expressed as the deflection in the direction of loading,

$$\Delta z = \delta \sin \theta = \frac{8WL^3 \sin^2 \theta}{3E_f \pi D^4}, \quad (4)$$

while the transverse (radial) deflection can be written as

$$\Delta r = \delta \cos \theta = \frac{8WL^3 \sin \theta \cos \theta}{3E_f \pi D^4}. \quad (5)$$

3.1.2. Elastic deformation of an isotropic bonded fibre array

The overall applied stress is related to the axial load on individual fibre segments by the equation

$$\sigma = NW, \quad (6)$$

where N is the number of fibre segments per unit sectional area. The relationship between N and f , the fibre volume fraction, depends on the fibre segment orientation distribution. For a 3D randomly oriented (isotropic) array of prisms, the area intersected by any plane is twice the area intersected by a plane lying normal to the alignment direction of a set of parallel prisms occupying the same volume fraction [19]. Hence, in this case N has a value of half that for the case of an aligned set of cylinders ($=f/(\pi D^2/4)$), i.e.,

$$N = \frac{2f}{\pi D^2}. \quad (7)$$

Substituting for W from Eqs. (6) and (7), the axial deflection is therefore given by

$$\Delta z = \frac{4\sigma L^3 \sin^2 \theta}{3E_f f D^2}, \quad (8)$$

and the transverse deflection by

$$\Delta r = \frac{4\sigma L^3 \sin \theta \cos \theta}{3E_f f D^2}. \quad (9)$$

The macroscopic deflection in the loading direction, and hence the strain, can be obtained by summing the contributions from the deflections of individual fibres. Doing this in a rigorous manner is clearly complex, since the deflections exhibited by individual fibre segments will be influenced by the configuration of neighbouring segments. However, if it is assumed that these interactions will, on average, have a negligible effect, at least for an isotropic, homogeneous material, then the net strain can be obtained by simple integration, taking into account that an isotropic fibre orientation distribution exhibits a $\sin \theta$ probability about any given axis:

$$\varepsilon_z = \frac{\Delta Z}{Z} = \frac{\int_0^{\pi/2} \Delta z \sin \theta d\theta}{\int_0^{\pi/2} z \sin \theta d\theta} = \frac{\int_0^{\pi/2} \frac{4\sigma L^3 \sin^3 \theta}{3E_f f D^2} d\theta}{\int_0^{\pi/2} \left(\frac{L}{2} \cos \theta \right) \sin \theta d\theta}, \quad (10)$$

$$\begin{aligned} \therefore \varepsilon_z &= \left(\frac{8\sigma}{3E_f f} \right) \left(\frac{L}{D} \right)^2 \frac{\int_0^{\pi/2} \sin^3 \theta d\theta}{\int_0^{\pi/2} \cos \theta \sin \theta d\theta} \\ &= \left(\frac{8\sigma}{3E_f f} \right) \left(\frac{L}{D} \right)^2 \frac{2/3}{1/2} = \left(\frac{32\sigma}{9E_f f} \right) \left(\frac{L}{D} \right)^2. \end{aligned} \quad (11)$$

The Young's modulus of the fibre array, $E_a (= \sigma/\varepsilon_z)$, is therefore given by

$$E_a = \frac{9E_f f}{32 \left(\frac{L}{D} \right)^2}. \quad (12)$$

The form of this prediction may be compared with that given by Gibson and Ashby [14] for an open cell foam. This is also based on beam deflections (3-point bending under a normal load, rather than the connected pair of inclined cantilevers assumed in the present model), but the geometry is more constrained. Assuming simply supported cylindrical beams lying parallel or normal to the applied load, the Young’s modulus predicted by the Gibson and Ashby model can be expressed in terms of L and D as follows:

$$E_a = \frac{3\pi E_f}{4\left(\frac{L}{D}\right)^4}. \tag{13}$$

Alternative assumptions regarding the constraint at the ends of the beam would lead to a higher predicted stiffness. It may be noted that in the Gibson and Ashby model the void content has a fixed relationship with the beam aspect ratio, whereas in the proposed model these can be independently specified. In practice there may at least be constraints on the combinations which are possible.

The transverse deflections can also be analysed, such that the strain is given by:

$$\begin{aligned} \varepsilon_r &= \frac{\Delta R}{R} = \frac{\int_0^{\pi/2} \Delta r \sin \theta \, d\theta}{\int_0^{\pi/2} r \sin \theta \, d\theta} \\ &= \left(\frac{8\sigma}{3E_f f}\right) \left(\frac{L}{D}\right)^2 \frac{\int_0^{\pi/2} \sin^2 \theta \cos \theta \, d\theta}{\int_0^{\pi/2} \sin^2 \theta \, d\theta}, \tag{14} \\ \therefore \varepsilon_r &= \left(\frac{8\sigma}{3E_f f}\right) \left(\frac{L}{D}\right)^2 \frac{1/3}{\pi/4} = \left(\frac{32\sigma}{9\pi E_f f}\right) \left(\frac{L}{D}\right)^2. \end{aligned}$$

The Poisson ratio, ν ($=\varepsilon_r/\varepsilon_z$) is thus predicted to have a constant value of $1/\pi$ (~ 0.32), independent of the fibre volume fraction and fibre segment aspect ratio. Since the material is isotropic, E_a and ν together fully define the elastic behaviour.

3.1.3. Onset of inelastic behaviour

The stresses within a cantilever beam are known, so it is a simple matter to predict the applied load at which the peak stress within the system will reach the yield stress of the fibre material. The maximum local stress will occur at the fibre surface, at the position along the beam where the bending moment reaches a peak (i.e., adjacent to the joints),

$$\sigma_{f,max} = \frac{D}{2} \frac{M}{I} = \frac{D}{2} \frac{W \sin \theta (L/2)}{(\pi D^4/64)}. \tag{15}$$

Neglecting any dependence of the axial load (W) on the fibre orientation, and substituting for the average value of W from Eqs. (6) and (7), the peak stress (for $\theta = 90^\circ$) can be expressed relative to the applied stress,

$$\sigma_{f,max} = \sigma_f \frac{8}{f} \left(\frac{L}{D}\right). \tag{16}$$

On setting this stress equal to the fibre yield stress, $\sigma_{f,Y}$, an estimate can be obtained of the applied stress at which inelastic behaviour might be expected to start,

$$\sigma_{a,Y} = \sigma_{f,Y} \frac{f}{8\left(\frac{L}{D}\right)}. \tag{17}$$

3.1.4. Effect of the presence of an environment (matrix)

There is interest in how the behaviour will be modified when material is introduced into the inter-fibre space, with attention primarily directed towards cases in which this material has a much lower stiffness than the fibre. While a fibre will clearly deflect less under the influence of a given applied load when surrounded by a matrix of finite stiffness, the form of the deflection–distance relationship along the length of the fibre will be the same (assuming that the matrix is elastically homogeneous and isotropic). This is illustrated in Fig. 4. In the absence of a matrix (Fig. 4(a)), the force $W \sin \theta$, effectively acting on the fibre mid-point, normal to the fibre axis, is counterbalanced by the force exerted by the elastically strained fibre, so that

$$W \sin \theta = \frac{3\pi D^4 E_f}{8L^3} \delta_{0,L/2}. \tag{18}$$

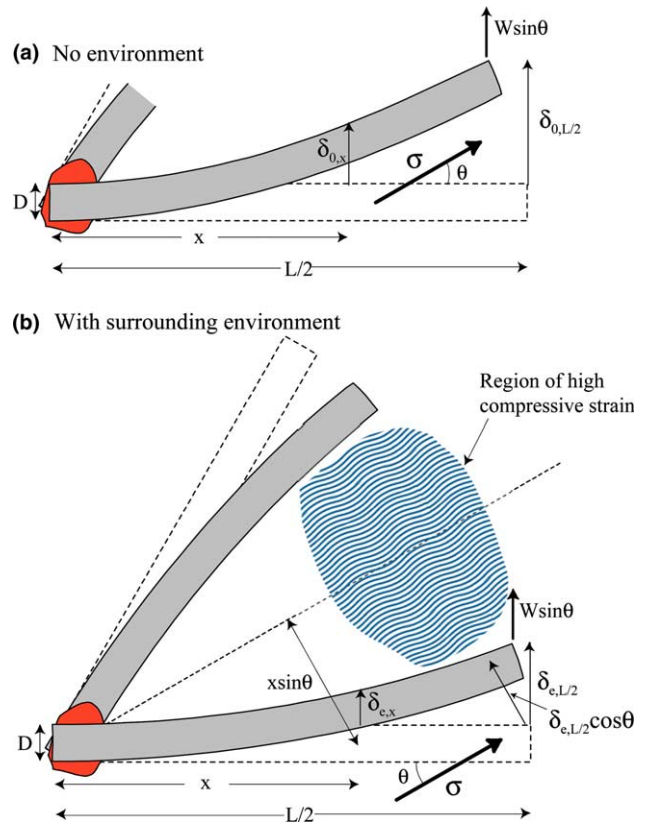


Fig. 4. Schematic representation of the elastic deformation of a bonded pair of fibres, with and without a surrounding environment of finite stiffness.

When an environment (matrix) is present, however, the deflection of the fibre mid-point, $\delta_{e,L/2}$, will be less than $\delta_{0,L/2}$ and the force exerted by the elastically strained fibre will be correspondingly reduced (Fig. 4(b)). The overall force balance is now satisfied by introduction of the force exerted on the fibre by the strained environment, which will vary along the length of the fibre. This balance can thus be expressed

$$W \sin \theta = \frac{3\pi D^4 E_f}{8L^3} \delta_{e,L/2} + \int_0^{L/2} P_x dx, \quad (19)$$

where P_x is the force per unit length of fibre, exerted on it by the environment. An expression for P_x can be written in terms of the stiffness of the environment, E_c the fibre diameter, D , the local fibre deflection, $\delta_{e,x}$, and the thickness of the environment over which this deflection is accommodated. The latter can, to a first approximation, be taken as half the inter-fibre spacing – see Fig. 4(b). Of course, this will vary with the local fibre orientation geometry, but a pair of fibres symmetrically disposed about the stress axis may be taken as a representative situation. Half the inter-fibre spacing is then given by $x \sin \theta$. The environment is presumably being compressed on one side of the fibre and stretched on the other side, so a factor of 2 should also be included. Finally, this force actually operates normal to the line bisecting the two fibres, rather than normal to the fibre axis, so a further factor of $\cos \theta$ is needed in order to implement Eq. (19). Acknowledging that some gross simplifications are being incorporated here, the expression required is therefore,

$$P_x \approx 2 \left(\frac{\delta_{e,x}}{x \sin \theta} \right) E_c D \cos \theta. \quad (20)$$

Substituting this expression into Eq. (19) gives

$$W \sin \theta = \frac{3\pi D^4 E_f}{8L^3} \delta_{e,L/2} + \int_0^{L/2} \left(\frac{2\delta_{e,x}}{x \tan \theta} \right) E_c D dx. \quad (21)$$

The fibre deflection at a distance x along its length is related to that at the fibre mid-point via the relationship,

$$\delta_{e,x} = \delta_{e,L/2} \left(\frac{3(\frac{L}{2})x^2 - x^3}{2(\frac{L}{2})^3} \right) = 2x^2 \left(\frac{3L - 2x}{L^3} \right) \delta_{e,L/2}, \quad (22)$$

so that, substituting this expression into Eq. (21) and integrating:

$$\begin{aligned} W \sin \theta &= \frac{3\pi D^4 E_f \delta_{e,L/2}}{8L^3} + \int_0^{L/2} \frac{4x^2 \left(\frac{3L-2x}{L^3} \right) \delta_{e,L/2} E_c D dx}{x \tan \theta}, \\ \therefore W \sin \theta &= \frac{3\pi D^4 E_f \delta_{e,L/2}}{8L^3} + \frac{4E_c D \delta_{e,L/2}}{L^3 \tan \theta} \int_0^{L/2} x(3L-2x) dx, \\ \therefore W \sin \theta &= \frac{3\pi D^4 E_f \delta_{e,L/2}}{8L^3} + \frac{7E_c D \delta_{e,L/2}}{6 \tan \theta}, \end{aligned} \quad (23)$$

which can be rearranged to give an expression for the deflection of the fibre mid-point, in the presence of an environment,

$$\delta_{e,L/2} = \frac{W \sin \theta}{\left(\frac{3\pi D^4 E_f}{8L^3} + \frac{7E_c D}{6 \tan \theta} \right)}. \quad (24)$$

The ratio of the deflections of the fibre mid-point (and also of any other point along the fibre length), with and without the environment present, is thus obtained after substituting finite and zero values for E_c into this equation,

$$\begin{aligned} \frac{\delta_{e,L/2}}{\delta_{0,L/2}} &= \frac{\frac{W \sin \theta}{\left(\frac{3\pi D^4 E_f}{8L^3} + \frac{7E_c D}{6 \tan \theta} \right)}}{\frac{W \sin \theta}{\left(\frac{3\pi D^4 E_f}{8L^3} \right)}} = \frac{1}{1 + \frac{28}{9\pi} \left(\frac{L}{D} \right)^3 \left(\frac{E_c}{E_f} \right) \cot \theta} \\ &= \frac{1}{1 + K \cot \theta}, \end{aligned} \quad (25)$$

in which K , given by

$$K = \frac{28}{9\pi} \left(\frac{L}{D} \right)^3 \left(\frac{E_c}{E_f} \right) \quad (26)$$

can be regarded as a ‘‘matrix stiffness factor’’.

This expression can now be used to predict the effect of the presence of the environment on the stiffness of the fibre array. A modified expression for the strain now incorporates a reduced fibre deflection term, such that:

$$\begin{aligned} \varepsilon_z &= \frac{\Delta Z}{Z} = \frac{\int_0^{\pi/2} \Delta z \sin \theta d\theta}{\int_0^{\pi/2} z \sin \theta d\theta} \\ &= \frac{\int_0^{\pi/2} \frac{4\sigma L^3 \sin^3 \theta}{3E_f D^2} \left(\frac{1}{1+K \cot \theta} \right) d\theta}{\int_0^{\pi/2} \left(\frac{L}{2} \cos \theta \right) \sin \theta d\theta}, \end{aligned} \quad (27)$$

$$\begin{aligned} \therefore \varepsilon_z &= \left(\frac{8\sigma}{3E_f f} \right) \left(\frac{L}{D} \right)^2 \frac{\int_0^{\pi/2} \left(\frac{\sin^3 \theta}{1+K \cot \theta} \right) d\theta}{\int_0^{\pi/2} \cos \theta \sin \theta d\theta} \\ &= \left(\frac{32\sigma}{9E_f f} \right) \left(\frac{L}{D} \right)^2 Q, \end{aligned} \quad (28)$$

in which Q is a strain reduction factor, given by

$$Q = \left(\frac{3}{2} \right) \int_0^{\pi/2} \left(\frac{\sin^3 \theta}{1+K \cot \theta} \right) d\theta. \quad (29)$$

This integral has no closed form solution, but it can be evaluated numerically. The dependence of Q on K is shown in Fig. 5. It can be seen that its value approaches unity as the matrix stiffness tends to zero, as expected.

The Young’s modulus E_c of a bonded fibre array surrounded by a medium with finite stiffness (i.e., a composite) can therefore be written as

$$E_c = \frac{9E_f f}{32 \left(\frac{L}{D} \right)^2 Q}. \quad (30)$$

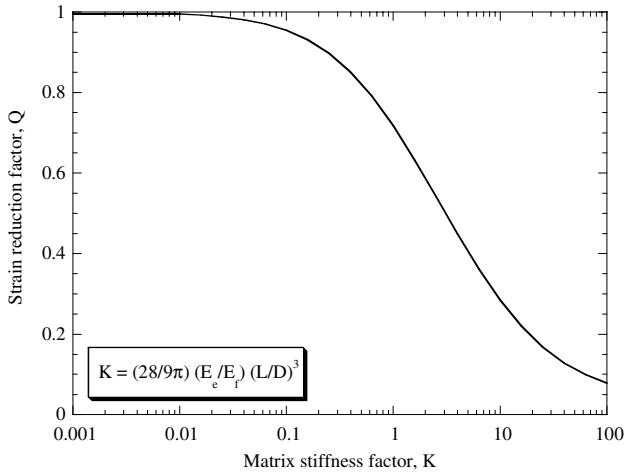


Fig. 5. Predicted dependence (Eq. (29)) on matrix stiffness factor of the strain reduction induced in a bonded-fibre porous material by the presence of a matrix.

Furthermore, using this model, the Poisson ratio is predicted to be unaffected by the presence of the matrix. It should be borne in mind that the model is only expected to be valid in cases where $E_e \ll E_f$ and $(L/D) \gtrsim 3$.

3.2. Magnetic loading

A magnetic load is generated by the application of a uniaxial magnetic field. This will always tend to generate an axial tensile strain in the fibre array, as a consequence of individual fibres becoming magnetised along their length and hence tending to line up parallel to the applied field. This is illustrated schematically in Fig. 6. Any effect on the net field experienced by an individual fibre, arising from the magnetisation of neighbouring fibres, is assumed to be small.

3.2.1. Individual fibre deflections

Fig. 7 depicts the elastic deformation of a single fibre, lying at an angle θ to the direction of the field. The tor-

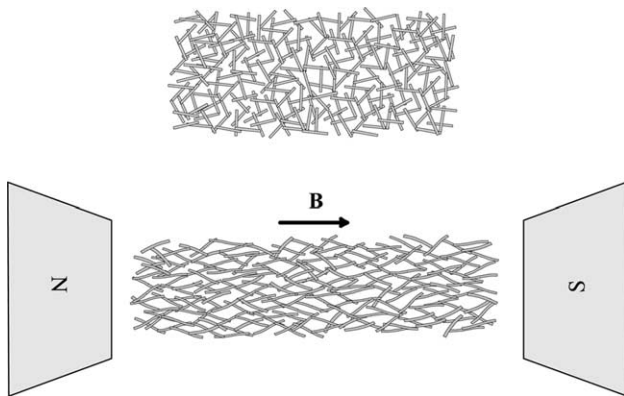


Fig. 6. Schematic representation of how a bonded array of randomly oriented magnetic fibres will deform in a magnetic field.

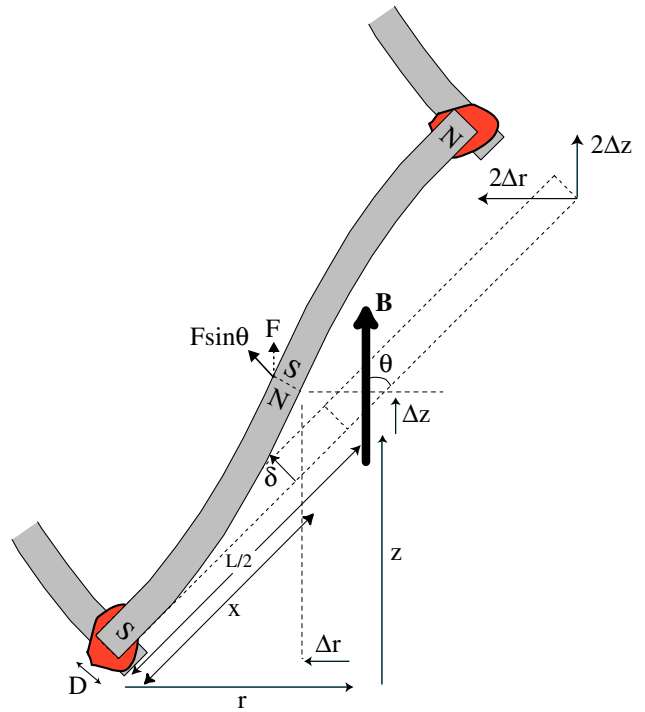


Fig. 7. Schematic representation of the deflection of a fibre segment within a fibre array, under the influence of an applied magnetic field, B .

que (bending moment) acting on a magnetic dipole lying in such a field (B) is given by

$$\text{torque} = (F \sin \theta)L = m \sin \theta B, \tag{31}$$

where F is the total force, effectively acting at the fibre end, and m is the dipole, which is related to the saturation magnetisation, M_s by

$$m = \frac{\pi D^2}{4} L M_s. \tag{32}$$

Again using the standard formula for the deflection of an end-loaded cantilever beam,

$$\delta = \frac{8M_s B \sin \theta}{3E_f D^2} (3Lx^2 - x^3), \tag{33}$$

leads to the following expressions for the deflections parallel and normal to the applied field, at a distance x along the length of the fibre:

$$\begin{aligned} \frac{\Delta z}{z} &= \frac{\delta \sin \theta}{x \cos \theta} \\ &= \frac{8M_s B \sin \theta \tan \theta}{3E_f} \left[3\left(\frac{x}{L}\right) - \left(\frac{x}{L}\right)^2 \right] \left(\frac{L}{D}\right)^2, \end{aligned} \tag{34}$$

$$\begin{aligned} \frac{\Delta r}{r} &= \frac{-\delta \cos \theta}{x \sin \theta} \\ &= \frac{-8M_s B \cos \theta}{3E_f} \left[3\left(\frac{x}{L}\right) - \left(\frac{x}{L}\right)^2 \right] \left(\frac{L}{D}\right)^2. \end{aligned} \tag{35}$$

The broad validity of these expressions have been confirmed experimentally [6] by comparing measured and

predicted deflections for single pieces of wire and for small welded assemblies.

3.2.2. Elastic deformation of isotropic bonded fibre array

Magnetically induced deformations (local and global) in a 3D fibre array can be predicted using a similar approach to that used for mechanical loading. The overall extension parallel to the applied field can be expressed by considering the displacements of a set of fibre mid-points (see Fig. 7)

$$\begin{aligned} \frac{\Delta Z}{Z} &= \frac{\int_0^{\pi/2} \Delta z \sin \theta d\theta}{\int_0^{\pi/2} z \sin \theta d\theta} \\ &= \frac{\int_0^{\pi/2} \frac{8M_s B}{3E_f D^2} \sin^2 \theta \left(3\left(\frac{L}{2}\right)^3 - \left(\frac{L}{2}\right)^3 \right) \sin \theta d\theta}{\int_0^{\pi/2} \left(\frac{L}{2} \cos \theta\right) \sin \theta d\theta} \\ \therefore \frac{\Delta Z}{Z} &= \frac{\frac{2M_s B L}{3E_f} \left(\frac{L}{D}\right)^2 \int_0^{\pi/2} \sin^3 \theta d\theta}{\frac{L}{4}} = \left(\frac{16M_s B}{9E_f}\right) \left(\frac{L}{D}\right)^2 \quad (36) \end{aligned}$$

The concept of “magnetic stiffness” of a bonded fibre array, $S_a (=B/\epsilon_z)$ may now be introduced. This represents the applied field required to generate unit elastic strain, in an analogous manner to the Young’s modulus representing the applied stress needed to generate unit elastic strain,

$$S_a = \frac{9E_f}{16M_s \left(\frac{L}{D}\right)^2}. \quad (37)$$

The transverse contraction is similarly derived:

$$\begin{aligned} \frac{\Delta R}{R} &= \frac{\int_0^{\pi/2} \Delta r \sin \theta d\theta}{\int_0^{\pi/2} r \sin \theta d\theta} \\ &= \frac{\int_0^{\pi/2} \frac{-8M_s B}{3E_f D^2} \sin \theta \cos \theta \left(3\left(\frac{L}{2}\right)^3 - \left(\frac{L}{2}\right)^3 \right) \sin \theta d\theta}{\int_0^{\pi/2} \left(\frac{L}{2} \sin \theta\right) \sin \theta d\theta}, \\ \therefore \frac{\Delta R}{R} &= \frac{\frac{-2M_s B L}{3E_f} \left(\frac{L}{D}\right)^2 \int_0^{\pi/2} \sin^2 \theta \cos \theta d\theta}{\frac{L}{8}} \\ &= \left(\frac{-16M_s B}{9\pi E_f}\right) \left(\frac{L}{D}\right)^2. \quad (38) \end{aligned}$$

This analysis can be used to predict how a porous specimen of this type would change shape on application of a magnetic field. For example, Fig. 8 shows axial and transverse strains expected on application of a magnetic field of strength 1.5 Tesla. It is clear that these deformations are sensitive to the aspect ratio (L/D) of the segments of fibre between joints. It can be seen that, with a high fibre aspect ratio (≥ 25), application of a field of this magnitude is predicted to generate quite substantial macroscopic strains ($\geq 1\%$). It may

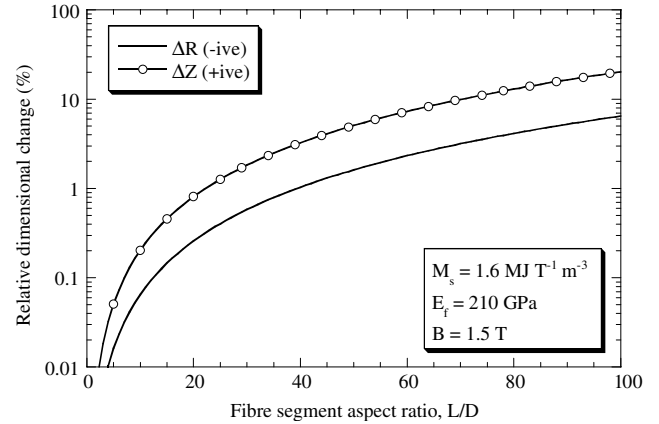


Fig. 8. Predicted dependence on fibre segment aspect ratio, according to Eqs. (36) and (38), of the dimensional changes induced in a bonded-fibre porous material by applying a magnetic field of strength 1.5 Tesla. Relevant fibre properties are indicated in the figure.

be noted that, while there is no explicit dependence on the fibre volume fraction in the material, this would normally have to be relatively low in order to allow such high fibre aspect ratios, particularly with a 3D random fibre array.

3.2.3. Onset of inelastic behaviour

The maximum fibre stress under magnetic loading can be related to the applied field, using a similar approach to that of Section 3.1.3,

$$\begin{aligned} \sigma_{f,\max} &= \frac{D M}{2 I} = \frac{D F \sin \theta(L/2)}{2 (\pi D^4/64)} \\ &= \frac{D B M_s (\pi D^2/4) \sin \theta(L/2)}{2 (\pi D^4/64)} \\ &= 4B M_s \sin \theta \left(\frac{L}{D}\right), \quad (39) \end{aligned}$$

so that, at $\theta = 90^\circ$, setting this stress equal to the fibre yield stress allows evaluation of the field needed to stimulate inelastic behaviour,

$$B_{a,Y} = \frac{\sigma_{f,Y}}{4M_s \left(\frac{L}{D}\right)}. \quad (40)$$

3.2.4. Effect of the presence of an environment (matrix)

The treatment of Section 3.1.4 also applies to magnetically induced straining, with the matrix assumed to be non-magnetic. The same strain reduction factor applies. The “magnetic stiffness” S_c of a bonded fibre array infiltrated with a matrix of finite stiffness is therefore given by

$$S_c = \frac{9E_f}{16M_s \left(\frac{L}{D}\right)^2 Q}. \quad (41)$$

4. Mechanical characteristics

Predicted relative stiffnesses are shown in Fig. 9, as a function of fibre segment aspect ratio, for the Gibson and Ashby model (Eq. (13)) and for the random fibre array model (Eq. (12)), with three fibre volume fractions. Also shown are measured stiffness values for free-standing bonded fibre arrays with different f and L/D values. (The fibre segment aspect ratios for the bonded fibre arrays were estimated from SEM micrographs, such as the one shown in Fig. 1). The Gibson and Ashby model predicts a sharper fall in stiffness with increasing L/D than the Markaki and Clyne model. However, increases in L/D would often be accompanied by reductions in fibre content, f , making the effective plot for the Markaki and Clyne model somewhat steeper than the individual curves. The experimental data do seem to fit fairly well with both models, but more systematic data, and in particular more accurate L/D measurements (perhaps from X-ray tomography), are needed to verify this.

Predicted stiffnesses for impregnated fibre arrays, according to Eq. (30), are shown in Fig. 10 as a function of E_c/E_f for three L/D ratios. Also included are experimental data for fibre arrays infiltrated with rubber or resin, having measured matrix/fibre stiffness ratios, E_c/E_f as indicated in the plot. It can be seen that the predicted value for the rubber-impregnated array is in good agreement with experiment, while for the resin-impregnated array the experimental value is considerably higher. The reason for this is not entirely clear, but it must be recognised that the model incorporates various approximations and it certainly breaks down as the matrix stiffness becomes relatively high.

The stress at the onset of inelastic behaviour, predicted by Eq. (17), is plotted in Fig. 11(a) as a function

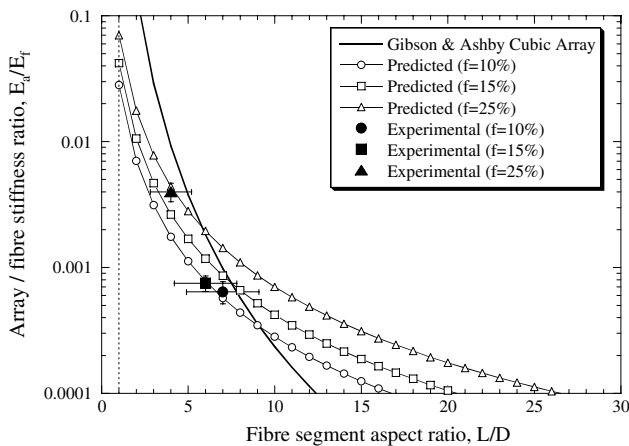


Fig. 9. Comparison between theory (Eq. (12)) and experiment for the relative stiffness of fibre arrays, with different fibre volume fractions. Also shown are predictions from the Gibson and Ashby model for a cubic array of fibres (Eq. (13)).

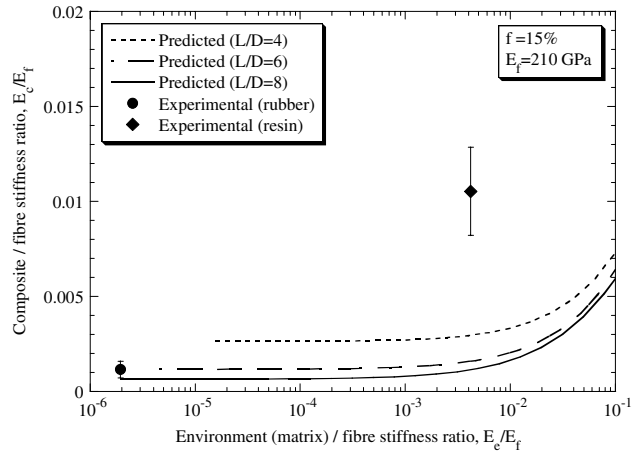


Fig. 10. Predicted dependence of the relative composite stiffness, E_c/E_f on the matrix/fibre stiffness ratio, E_c/E_f according to (Eq. (30)), for different segment aspect ratios. Also shown are experimental data for fibre arrays impregnated with resin and rubber.

of L/D ratio, for fibre arrays with different fibre contents. Also included on this plot are measured values, taken as stress levels at the onset of the plateau regime in

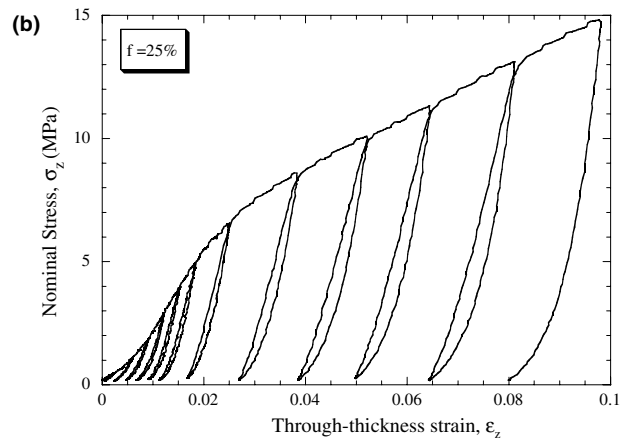
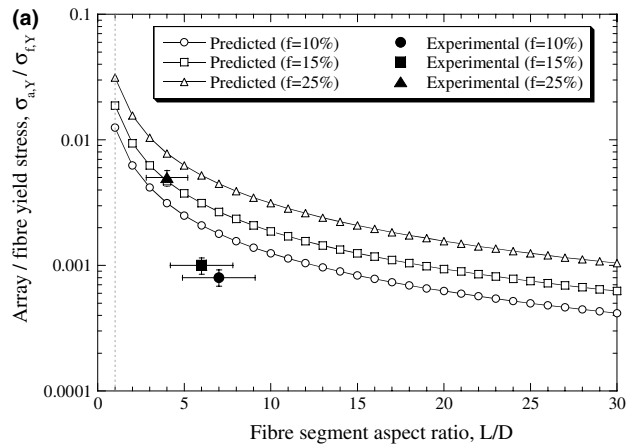


Fig. 11. (a) Predicted stress at the onset of inelastic behaviour of fibre arrays, as a function of segment aspect ratio, for different fibre volume fractions. Also shown are corresponding experimental data. (b) A typical stress–strain plot, for compressive testing of a fibre array with $f = 25\%$.

the stress–strain curve. A typical stress–strain curve is shown in Fig. 11(b). (The yield strength of the fibre ($\sigma_{f,Y} = 1000$ MPa) was obtained from single fibre testing [11].) It can be seen that the experimental data are broadly consistent with predictions from the model, although there are clearly difficulties in detecting plastic flow reliably.

5. Magneto-mechanical characteristics

The response to the application of a magnetic field of both free-standing fibre arrays and those infiltrated with rubber or resin is illustrated in Fig. 12. The plots show

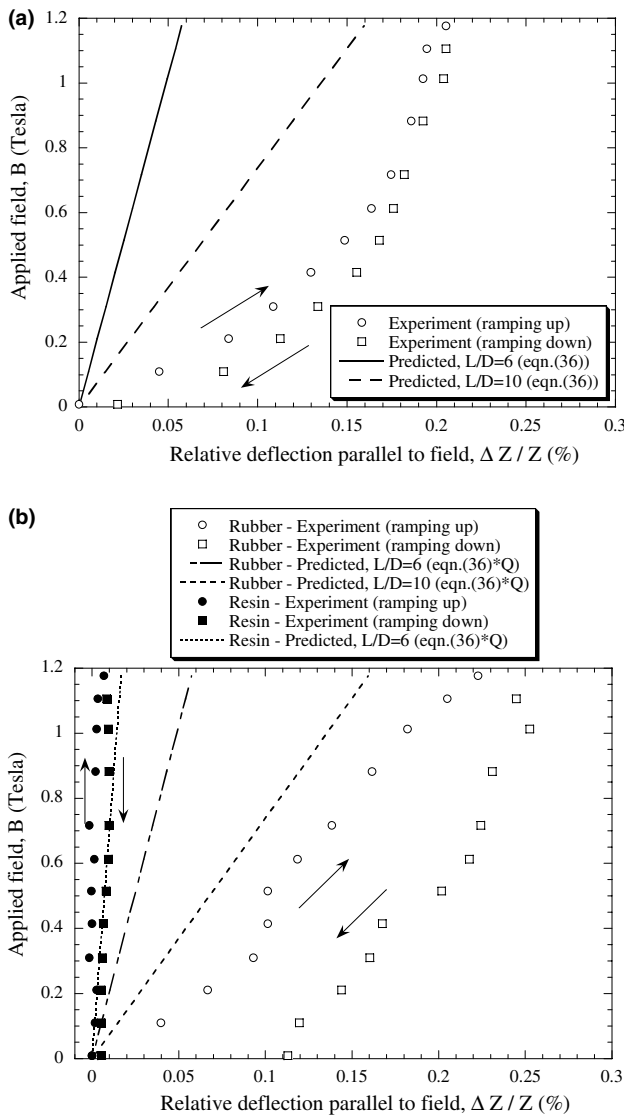


Fig. 12. Comparison between theory and experiment (scanning laser extensometer data) for the change in length as a function of field strength for: (a) a free-standing fibre array and (b) fibre arrays infiltrated with rubber and resin.

relative length changes of the specimens, as a function of the applied magnetic field. The field was ramped up and down, with a maximum value of about 1.2 Tesla. Length changes approaching 0.2% were recorded for the free-standing fibre array (Fig. 12(a)) and the array infiltrated with rubber (Fig. 12(b)), whereas for the resin-impregnated array (Fig. 12(b)), the straining was barely detectable. The latter is unsurprising, since the strains are reduced as the constraint imposed by the surrounding material increases. The rate of strain increase drops at higher field strengths. This is probably a geometric effect, since the fibre deflections will approach saturation at high fields and the predicted deflections refer only to the low strain regime. Furthermore, it can also be seen that there is some hysteresis, with the induced length change not being entirely reversible on reducing the applied field. This may be due to formation of fibre entanglements, which persist after removal of the field. This effect appears more pronounced for the rubber-impregnated array, which may be attributable to creep deformation of the rubber. It seems unlikely that any plastic deformation occurred in the fibres during these experiments: according to Eq. (40), field strengths of about 25 Tesla would be needed to induce this.

Comparison between measured and predicted changes shows that, for the non-impregnated and the rubber-impregnated arrays, the measured deflections are larger than those predicted by the model. While close agreement with experiment is not really expected here, since in reality the deformation behaviour of a fibre network is expected to be complex, it is important to note that these predictions are very sensitive to the segment aspect ratio. This is illustrated in Fig. 12,

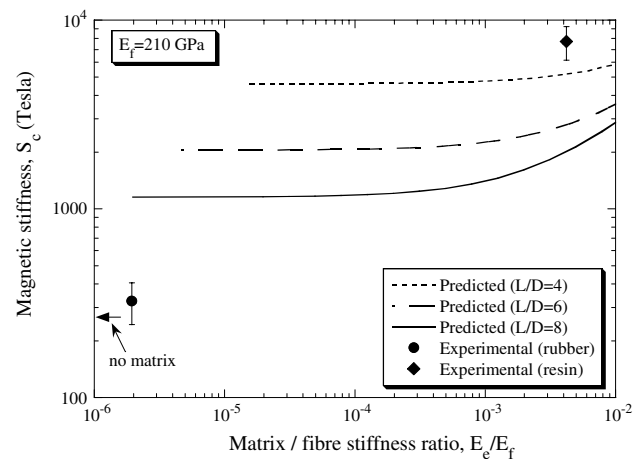


Fig. 13. Predicted dependence on the matrix/fibre stiffness ratio, E_e/E_f of the magnetic stiffness, S_c (Eq. (41)), of arrays with different segment aspect ratios. Also shown are experimental data for fibre arrays with and without a surrounding matrix.

which shows predicted shape changes as a function of the applied magnetic field, for two segment aspect ratios. The value of 6 used for the prediction was estimated from micrographs such as those shown in Fig. 1. Predictions are also shown for a segment aspect ratio of 10, since it is possible that not all the fibres are bonded at their cross-over points. Clearly, more accurate measurement of L/D is needed and X-ray tomography experiments are currently being conducted, with this objective.

Fig. 13 shows predicted magnetic stiffnesses of impregnated fibre arrays, according to Eq. (41), as a function of the matrix/fibre stiffness ratio, for three fibre volume fractions. The experimental values are taken from the low strain gradient of the plots in Fig. 12. Again, the agreement is reasonable, given the crude nature of the model.

6. Conclusions

This paper relates to material comprising an assembly of metallic fibres, bonded at contact points between them, with or without a relatively compliant matrix filling the inter-fibre space. It is aimed at generating an analytical framework within which to study and develop such materials. An experimental and theoretical investigation has been carried out into their behaviour in response to uniaxial mechanical loading and, for the case of the fibres being ferromagnetic, to an applied magnetic field. In the latter case, deformation results from the tendency for (magnetised) fibres to align with the direction of the applied field. The work is oriented towards material in which the fibre orientation distribution is random, although the approaches presented are applicable to other cases. The following conclusions can be drawn.

- (a) Simple analytical models have been developed to predict the mechanical response of the material, when subjected to either mechanical or magnetic forces. These models are based on the assumption that the deformation is dominated by bending of individual fibres, with any dimensional changes induced directly by the applied load or field being negligible in comparison. These models are therefore applicable only to cases in which the fibre segments (between joints) are relatively slender ($L/D \gtrsim 3$) and any matrix present is much more compliant than the fibre material. A further key assumption is that the net dimensional changes exhibited by the material can be obtained via a simple integration procedure, summing the deflections which would be exhibited by individual fibres if they were free-standing.
- (b) An expression has been derived for the Young's modulus of such material, relative to that of the fibres, as a function of the fibre segment aspect ratio, L/D , and the fibre volume fraction, f . The form of this prediction is similar to that of a previously developed expression (Gibson and Ashby model) based on a regular, orthogonal set of fibres, except that L/D and f can be independently specified in the current model and the predicted dependence on aspect ratio is rather less sharp. Comparisons with experiment are limited, partly because of difficulties in reliably estimating L/D , but are nevertheless encouraging.
- (c) The effect of the presence of a (compliant) matrix has been simulated in the model by introducing some crude assumptions about how its presence will inhibit fibre bending. This leads to an expression for a "strain reduction factor", which is dependent on a "matrix stiffness factor" involving L/D and the matrix/fibre stiffness ratio. The resulting predictions are at least broadly consistent with some very limited experimental data obtained in the current work.
- (d) The onset of plastic deformation has also been modelled, by comparing peak stresses within the fibres with the nominal yield stress of the fibre material. Again, reasonable agreement has been observed with experiment, although the comparison is hindered by difficulties in reliably detecting this onset.
- (e) Predictive equations have also been developed, using the same type of model, for the elastic deformation induced by imposition of a magnetic field. The concept of a "magnetic stiffness", S , is introduced, analogous to a Young's modulus, E , in the sense that it is the applied magnetic field needed to induce unit elastic strain, whereas E is the applied stress needed to induce unit elastic strain. The expression for S incorporates the saturation magnetisation of the fibre material, as well as the fibre Young's modulus and the fibre segment aspect ratio.
- (f) Measured magnetic stiffness values, taken from the initial gradient of a plot of applied field against induced strain, are in fairly good agreement with model predictions. A tendency was observed for the induced strain to saturate at high applied fields, but this non-linearity is expected as a result of geometry changes as individual fibre deflections become relatively large. Some hysteresis was also observed, leaving small residual strains at zero field. This may be attributable to fibre entanglements. In general, the magneto-mechanical model seems to be broadly applicable to 3D random arrays of ferromagnetic fibres and it should prove useful, at least as a starting point, during any development of devices based on such effects.

Acknowledgements

Financial support for this work has come from the Cambridge-MIT Institute (CMI) and from EPSRC, via a platform grant. The authors are grateful to Dr. Igor Golosnoy, for help with parts of the modelling work and Dr. Bartek Glowacki, of the Device Materials Group, for cooperation regarding the magnetic measurements. The fibres were supplied by Lee Marston and Peter Rooney, of Fibretech, with whom extensive ongoing collaboration is taking place.

Appendix A. Nomenclature

Symbols

B	applied magnetic field strength (T)
D	fibre diameter (m)
E	Young's modulus (Pa)
f	fibre volume fraction (–)
F	magnetically induced force, effectively acting on fibre end (N)
I	second moment of area of fibre section (m ⁴)
K	matrix stiffness factor (–)
L	fibre length (m)
m	magnetic dipole (J T ⁻¹)
M	magnetisation (J T ⁻¹ m ⁻³)
N	number of fibres intersecting unit sectional area (m ⁻²)
P	force per unit length (N m ⁻¹)
Q	strain reduction factor (–)
R	length of fibre array in radial direction (m)
S	magnetic stiffness of fibre array (T)
W	force acting on fibre, along loading axis (N)
x	distance along fibre (m)
Z	length of fibre array in direction of applied load or field (m)
Δr	deflection of fibre mid-point in radial direction (m)
ΔR	net deflection of fibre array in radial direction (m)
Δz	deflection of fibre mid-point in direction of applied load or field (m)
ΔZ	net deflection of fibre array in direction of applied load or field (m)
δ	lateral deflection of a fibre (m)
ε	strain (–)
ν	Poisson ratio of fibre array (–)
θ	angle between loading (or field) axis and fibre axis (rad)
σ	stress (Pa)

Subscripts

0	in absence of matrix (environment)
a	fibre array

c	composite (fibre array with matrix)
e	in presence of matrix (environment)
f	fibre
$L/2$	at a distance $L/2$ along fibre length
max	maximum
r	in direction transverse to applied load or field
S	saturation
x	at a distance x along fibre length
Y	yield
z	in direction of applied load or field

References

- [1] Ducheyne P, De Meester P, Aernoudt E. Isostatically compacted metal fibre porous coatings for bone ingrowth. *Powder Metall Int* 1979;11(3):115–9.
- [2] Gibson LJ. Properties and applications of metallic foams. In: *Comprehensive composite materials*. In: Clyne TW, editor. *Metal matrix composites*, vol. 3. Amsterdam: Elsevier; 2000. p. 821–32.
- [3] Gibson LJ. Mechanical behaviour of metallic foams. *Ann Rev Mater Sci* 2000;30:191–227.
- [4] Banhart J. Manufacture, characterisation and application of cellular metals and metal foams. *Progress Mater Sci* 2001;46:559–632.
- [5] Bhattacharya A, Calmidi VV, Mahajan RL. Thermophysical properties of high porosity metal foams. *Int J Heat Mass Tran* 2002;45(5):1017–31.
- [6] Markaki AE, Clyne TW. Magneto-mechanical stimulation of bone growth in a bonded array of ferromagnetic fibres. *Biomaterials* 2004;25(19):4805–15.
- [7] Clyne TW, Mason JF. The squeeze infiltration process for fabrication of metal matrix composites. *Metall Trans A* 1987;18:1519–30.
- [8] Ducheyne P, Aernoudt E, De Meester P. The mechanical behaviour of porous austenitic stainless steel fibre structures. *J Mater Sci* 1978;13:2650–8.
- [9] Markaki AE, Clyne TW. Mechanics of thin ultra-light stainless steel sandwich sheet material: part I – stiffness. *Acta Mater* 2003;51(5):1341–50.
- [10] Markaki AE, Clyne TW. Mechanics of thin ultra-light stainless steel sandwich sheet material: part II – resistance to delamination. *Acta Mater* 2003;51(5):1351–7.
- [11] Markaki AE, Gergely V, Cockburn A, Clyne TW. Production of a highly porous material by liquid phase sintering of short ferritic stainless steel fibres and a preliminary study of its mechanical behaviour. *Comp Sci Techn* 2003;63:2345–51.
- [12] Delannay F, Clyne TW. Elastic properties of cellular metals processed by sintering mats of fibres. In: *MetFoam '99*. Bremen, Germany: Verlag MIT Publishing; 1999.
- [13] Delince M, Delannay F. Elastic anisotropy of a transversely isotropic random network of interconnected fibres: non-triangular network model. *Acta Mater* 2004;52:1013–22.
- [14] Gibson LJ, Ashby MF. *Cellular solids, structure and properties*. 2nd ed. Cambridge University Press; 1997.
- [15] Ashby MF, Evans AG, Fleck NA, Gibson LJ, Hutchinson JW, Wadley HNG. *Metal foams: a design guide*. Boston: Butterworth-Heinemann; 2000.
- [16] Delannay F. Elastic model of an entangled network of interconnected fibres accounting for negative Poisson ratio behaviour

- and random triangulation. *Int J Solids and Structures*, [in press].
- [17] Yamada Y, Wen CE, Chino Y, Shimojima K, Hosokawa H, Mabuchi M. Processing and mechanical properties of open-cell Mg Alloys. *Mat Sci Forum* 2003;419:1013–8.
- [18] Woesz A, Stampfl J, Fratzl P. Cellular solids beyond the apparent density – an experimental assessment of mechanical properties. *Adv Eng Mater* 2004;6(3):134–8.
- [19] Underwood EE. *Quantitative stereology*. Reading: Addison-Wesley Publishing Company; 1970.